Materials Advances

ROYAL SOCIETY OF CHEMISTRY

PAPER

View Article Online
View Journal | View Issue

Cite this: *Mater. Adv.*, 2023, 4, 5730

Enhancing the sensitivity of a water stable MOF as a H_2S gas sensor by the fabrication of a mixed-matrix membrane†

Mouli Das Dawn,[a] Karabi Nath,[a] Subhajit Saha,[a] Pritam Kumar Roy,[b] Mahitosh Mandal[b] and Kumar Biradha *[a]

Received 8th September 2023,
Accepted 10th October 2023

DOI: 10.1039/d3ma00681f

rsc.li/materials-advances

Hydrogen sulfide (H_2S) is a smelly, colorless, and hazardous gas even at sub-ppm level, produced predominantly from natural and anthropogenic sources. It is also called a 'knock-down gas' as its inhalation at higher concentrations can cause death. Therefore, several researchers are working on designing sensors with high stability and robustness for the real-time detection of H_2S gas. Apart from many other materials, metal–organic framework (MOF)-based fluorescent probes are of high interest for the detection of H_2S. Herein, we present a cost-effective acryl-amide functionalized 2D **Zn-bdc** MOF, which was shown to function as an excellent probe for the real-time detection of H_2S in liquid as well as in the gaseous form through a nucleophilic addition mechanism to olefinic bonds of the MOFs. Interestingly, in the aqueous phase, **Zn-bdc** was found to exhibit turn-off and subsequent turn-on fluorescence spectra with the gradual addition of H_2S. Furthermore, the realistic sensing of H_2S by the MOF was investigated by preparing a mixed-matrix membrane of MOF with PVDF as a binder. Notably, the membrane with 60% loading of **Zn-bdc** increased the probe's sensitivity by two-fold. Furthermore, we note that this is the first example of an essential metal based mixed-matrix membrane for H_2S detection with the LOD value as low as 5.3 μM. *In vitro* cell imaging of **Zn-bdc** in the presence of H_2S displays a vibrant bright red fluorescence signal of LN-18 glioblastoma cells.

Introduction

A recent upsurge in the development of thin-film based sensors for detecting toxic gases such as H_2S, CO_2, SO_2, NH_3, and NO_2 has drawn rigorous attention given their industrial applications.[1,2] Among these gases, hydrogen sulfide (H_2S) is a flammable, colorless, and deadly poisonous gas with the odour of rotten eggs and plays an effective role as a hazardous chemical in the environment.[3] H_2S is released into the environment as a by-product through various industrial processes in the chemical and pharmaceutical industries of natural gas production, petroleum refining and drilling, and also by the decomposition of sulfur-containing bio-molecules.[4] In mammals, the endogenous concentration of H_2S normally is at 10–100 micromolar level.[5] The deregulation of endogenous concentration of H_2S in the human body causes various types of diseases like Alzheimer's, Parkinson's, diabetes, and cancer.[6,7] In addition to this, prolonged exposure to H_2S vapor in a healthy body may also cause irritation of the eyes, nausea, headaches, respiratory failure, conjunctivitis, loss of sleep, and even death. Thus, the detection of H_2S in its gaseous phase is just as important as in the solution phase. Therefore, it is essential to develop a quantitative technique for the fast, selective, and sensitive detection of exogenous as well as endogenous H_2S in solution and in the gaseous phase. In this context, fluorescent H_2S probes are advantageous over other conventional techniques,[8–12] given their rapid response, simplicity in implementation, cell permeability, economic friendliness, and suitability for real-time detection.[13–17] To date, three fundamental strategies are in use for the development of fluorescent H_2S probes based on their reaction with H_2S: (a) reductive reaction with H_2S: reduction of nitro or azide to amine, and reduction of selenoxide to selenide; (b) nucleophilic addition reaction by H_2S: Michael addition reactions, addition to double bonds, dual nucleophilic reactions and thiolysis reactions; (c) precipitation reactions by H_2S as Hg^{2+}/Cu^{2+}/Au^{2+}/Ag^{+} sulfides.[18–24]

[a] *Department of Chemistry, Indian Institute of Technology Kharagpur, Kharagpur 721302, India. E-mail: kbiradha@chem.iitkgp.ac.in*
[b] *School of Medical Science and Technology, Indian Institute of Technology, Kharagpur 721302, India*

† Electronic supplementary information (ESI) available: Synthesis of BP3YF, Synthesis of MOF, Membrane preparation, XRPD patterns, TGA analysis, XPS plot, FTIR, ^{1}H-NMR data, cytotoxicity assay analysis, and a comparison table of H_2S sensing by MOFs. CCDC 2282228–2282230. For ESI and crystallographic data in CIF or other electronic format see DOI: https://doi.org/10.1039/d3ma00681f

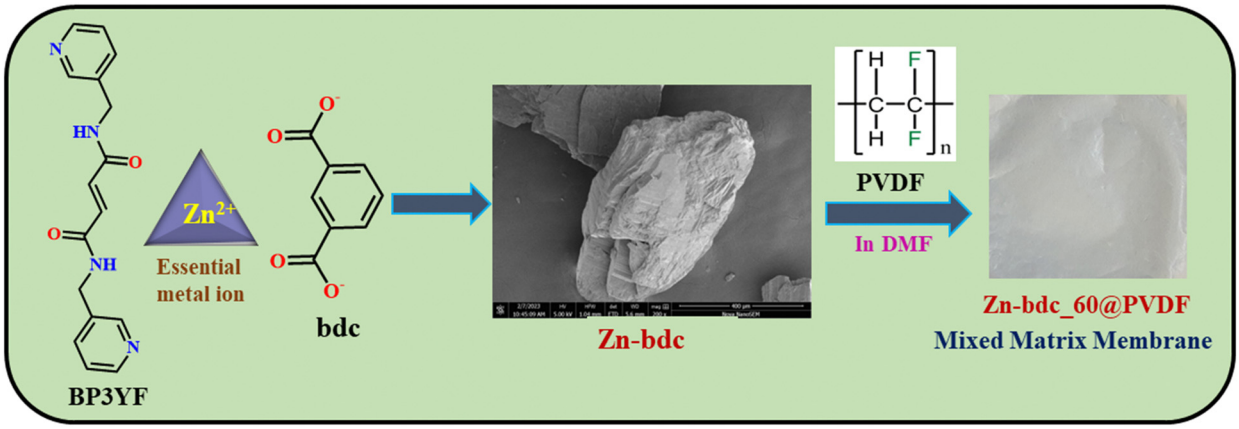

Scheme 1 Chemical structures of the ligand, metal, and ancillary ligand of **Zn-bdc** with FESEM image and preparation of the mixed-matrix membrane of **Zn-bdc_60@PVDF**.

Coordination polymers (CPs)/metal–organic frameworks (MOFs) have been at the center of attraction over the last two decades owing to their multi-dimensional applications in gas separation and storage,[25–29] guest inclusion,[30] proton conductivity,[31] sensing,[32–37] magnetism,[38] and catalysis.[39,40] MOFs are considered for these applications given their high thermal, and chemical, stability, large porosity, tunable surface area, and amenability for post-synthetic modifications. One of the most developing applications of MOFs is associated with selective sensing of various analytes such as anions, cations, nitro-aromatics, and biological signaling molecules like H_2S with very low detection limits.[41–44] In very recent years, post-synthetic modification of the functional groups on the well-known MOFs for the detection of H_2S has been shown as an efficient methodology (Table S5, ESI†). In this regard, vinyl functionalized MOFs of UiO-66 and CAU-10 were demonstrated for their ability in quantitative detection of H_2S in physiological conditions, which occurs through nucleophilic addition reaction of H_2S to the vinyl groups of MOFs.[45,46] Further, Huang and co-workers reported malononitrile functionalized UiO-66-NH-BQB MOF for the detection of H_2S and cysteine simultaneously.[47,48] Recently, we have shown the importance of nitro and azide groups containing Zn-CPs for the detection of H_2S by following the reductive reaction strategy.[49] Among all the three mentioned methodologies, the synthesis of a fluorescent H_2S probe based on nucleophilic addition reaction to the olefinic double bond of MOFs is very scarce. For the realistic sensing application of MOFs as a device, it is essential to fabricate their powder forms into thin-film membranes, which is not well explored to date. One such type of reported example is flexible Al-MIL-53-NO_2 MOF-based mixed-matrix membranes used as an H_2S sensor following the reductive reaction mechanism from the nitro to azide group.[50]

In this endeavor, we wish to present three Zn(II) MOFs (**Zn-bdc**, **Zn-cpb**, **Zn-btc**) containing acryl-amide functionalized organic struts, which have the propensity to detect H_2S in the solution state as well as in the gaseous state by undergoing the nucleophilic addition reaction. Until now, most of the MOF-based probes have been explored for H_2S detection either in the solution or gaseous phases.[51–55] Interestingly, in the aqueous phase, **Zn-bdc** was found to show turn-off and subsequent turn-on fluorescence responses with the gradual addition of H_2S and proved to be a better probe than **Zn-cpb** and **Zn-btc** in terms of stability, sensitivity, selectivity, and low response time with the detection limit of 10.7 μM. However, for real-time sensing applications using a thin-film based mixed-matrix membrane as a fluorescent H_2S probe has not yet been fully established. Taking this into account, we synthesized mixed-matrix membranes with highly stable 2D MOF **Zn-bdc** as a filler and poly(vinylidene fluoride) (PVDF) as a binder (Scheme 1). This mixed-matrix membrane was shown to exhibit turn-on fluorescence emission upon exposure to H_2S vapor following the nucleophilic addition reaction. The limit of detection (LOD) value of the **Zn-bdc** composite membranes was found to be reduced by 2 times compared to the dispersed aqueous phase of **Zn-bdc** MOF. In addition, **Zn-bdc_60@PVDF** is the first reported essential metal-based mixed-matrix membrane for H_2S detection with the lowest LOD value of 5.3 μM.

Results and discussion

BP3YF was synthesized by a simple condensation reaction of 3-(aminomethyl)pyridine and fumaric acid (Scheme S1, ESI†).[56] It was reported by our group earlier that the CPs composed of BP3YF function as adsorbents of oxoanion pollutants and toxic dyes.[57] The complexation reactions were conducted in solvothermal conditions by reacting **BP3YF** with three polycarboxylates such as flexible 4-(4′-carboxyphenoxy)benzoic acid (H_2cpb), angular benzene-1,3-dicarboxylic acid (H_2bdc), and rigid benzene-1,2,4,5-tetracarboxylic acid (H_4btc) with an essential metal $Zn(NO_3)_2$. These reactions produced single crystals of $\{[Zn(BP3YF)(cpb)]\}_n$, (**Zn-cpb**), $\{[Zn(BP3YF)(bdc)]\}_n$, (**Zn-bdc**), and $\{[Zn_2(BP3YF)(btc)(H_2O)_2]\}_n$, (**Zn-btc**) (Scheme S2, ESI†). **Zn-cpb** and **Zn-bdc** contain dicarboxylate as an ancillary

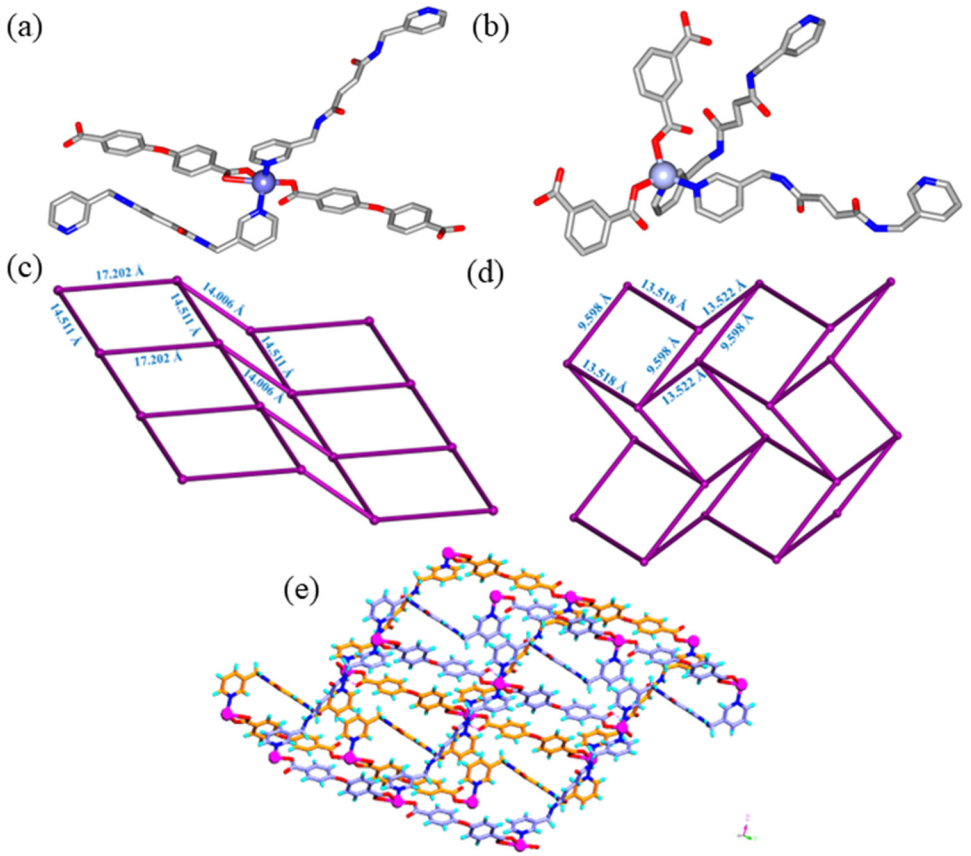

Fig. 1 (a) Coordination environment around the Zn metal centers of **Zn-cpb**; (b) coordination environment around the Zn metal centers of **Zn-bdc**; (c) node connected view of the corrugated 2D-layer in **Zn-cpb**; (d) formation of the node connected corrugated 2D-layered architecture of **Zn-bdc**; (e) packing of the layers of a **Zn-cpb** due to N–H···O interactions.

ligand and resulted in 2D corrugated networks, whereas **Zn-btc** with tetra carboxylate forms a 3D-network. The relevant crystallographic details, selected bond lengths, bond angles, and geometrical parameters of hydrogen bonding of **Zn-cpb**, **Zn-bdc**, and **Zn-btc** are shown in Tables S1, S2 and S4 (ESI†).

Single crystal X-ray diffraction analysis revealed that **Zn-cpb** and **Zn-bdc** crystallized in the $P\bar{1}$ and $P2_1/c$ space groups, respectively. The asymmetric unit in **Zn-cpb** is composed of two half units of **BP3YF**, one unit each of **cpb** and a Zn(II) ion and that of **Zn-bdc** is composed of one unit of **BP3YF**, **bdc**, and Zn(II) metal centers. The Zn(II) central ion adopts distorted square pyramidal coordination geometry in **Zn-cpb** as it coordinates two pyridine units of **BP3YF** and two **cpb** units, one of which forms chelation (Fig. 1a). In **Zn-bdc**, the Zn(II) metal centers exhibit distorted tetrahedral geometry as they coordinated to two pyridyl units of **BP3YF** and two carboxylates of the **bdc** unit (Fig. 1b). In both structures, Zn(II) ions with the carboxylate of **cpb**/**bdc** form a wavy one-dimensional chain (Fig. S1a, ESI†). These one-dimensional chains are further connected through the ligand **BP3YF** that results in the formation of the corrugated 2D network in both **Zn-cpb** and **Zn-bdc**. In **Zn-cpb**, the 2D-network contains rectangular (14.511 × 17.202 Å) as well as square cavities (14.511 × 14.006 Å) (Fig. 1c and S1b). Whereas the 2D-layers of **Zn-bdc** contain only rectangular cavities (9.592 × 13.522 Å) (Fig. 1d and Fig. S1c, ESI†). These 2D corrugated layers are packed on each other *via* N–H···O (N···O: 2.8162.826 Å, 159°, 170° in **Zn-cpb** and N···O: 2.30 Å, 177° in **Zn-bdc**) hydrogen bonds (Fig. 1e).

The **Zn-btc** MOF crystallized in the $P\bar{1}$ space group and the asymmetric unit is composed of one unit of Zn(II) ion, half units each of coordinated **BP3YF** and **btc**, and one coordinated water molecule. The Zn(II) metal center in **Zn-btc** adopts a distorted trigonal bipyramidal geometry where the two apical positions are occupied by carboxylate ions and coordinated water molecules whereas the three equatorial positions are occupied by two carboxylate O-atoms and one pyridyl unit (Fig. S1d, ESI†). The Zn(II) metal center and **btc** units by connecting with each other, resulted in a neutral 2D layer (Fig. 2a). The layers are formed by a bimetallic secondary building unit in which Zn(II) centers are separated by 3.336 Å, and capped by two carboxylates in a μ_2-bridging fashion. The 2D-layers are further pillared by **BP3YF** to generate a 3D-network (Fig. 2b) containing interlayer separation of 12.095 Å. The amide N–H groups form N–H···O hydrogen bonding with the carboxylate O atoms of **btc** (N–H···O, 1.92 Å; N···O, 2.827 Å, 154.79°).

In order to examine the H_2S sensing abilities of MOFs in water, the stability of the MOFs was investigated by immersing them in an aqueous medium for seven days. Comparison of the

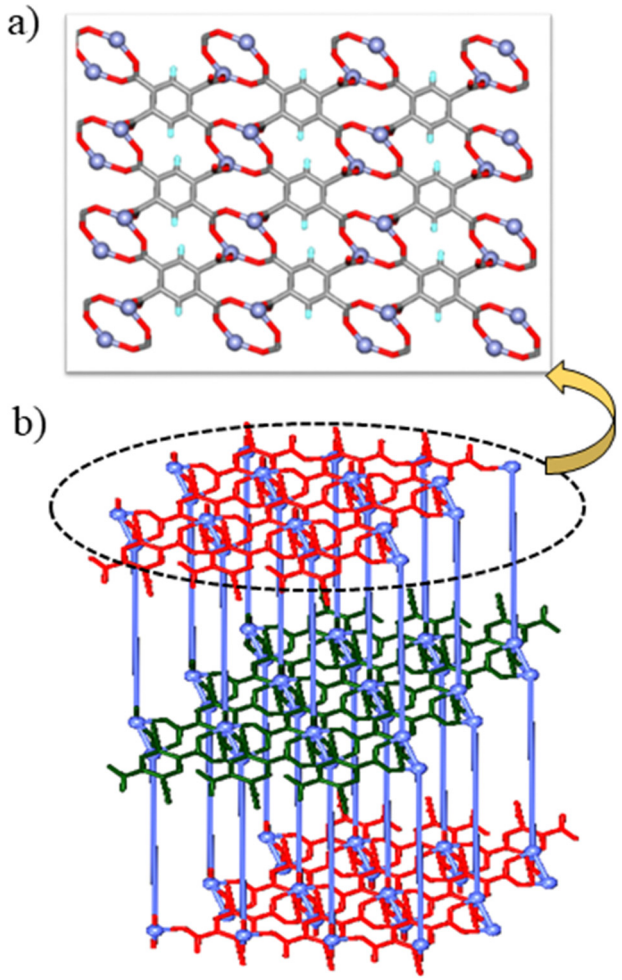

Fig. 2 (a) Formation of a 2D-layer by metal centers and btc moieties; (b) connection of the 2D-layers *via* the **BP3YF** ligand as pillars to generate the overall 3D-network.

XRPD patterns of the immersed samples with those of crystallized samples confirmed that two of the three MOFs, namely **Zn-bdc** and **Zn-btc**, are stable in water (Fig. S5, ESI†). The thermal stability of the MOFs was also checked by thermogravimetric analysis (TGA) (Fig. S6, ESI†). **Zn-cpb** and **Zn-bdc** are thermally stable up to 460 °C and 420 °C, respectively. In the case of **Zn-btc**, the initial 8% weight loss was observed at about 203 °C due to the loss of two coordinated water molecules and the network was found to be stable up to 481 °C. Prior to sensing studies, the solid-state luminescence properties of three MOFs and ligand **BP3YF** were examined at room temperature (Fig. S8, ESI†). **BP3YF** and all three MOFs have exhibited a luminescence emission maximum at ~460 nm (λ_{ex} = 290 nm), which can be attributed to $\pi \rightarrow \pi^*$ or $n \rightarrow \pi^*$ transitions due to Ligand-to-Ligand Charge Transfer (LLCT).[58] The solution state absorbance spectra of **BP3YF**, **Zn-cpb**, **Zn-bdc**, and **Zn-btc** display a peak around 290 nm wavelength (Fig. S7b, ESI†).

H_2S sensing in the dispersed aqueous phase

Interestingly, preliminary investigations on H_2S sensing in aqueous solutions of MOFs have indicated that they exhibit initial turn-off and subsequent turn-on fluorescence with the gradual addition of aq. Na_2S solution. The stock solutions of the MOFs (100 μM) were prepared by dispersing the finely ground samples in water such that a uniform suspension was formed. The aqueous solution of **Zn-bdc** was found to exhibit fluorescence at 405 nm with an excitation wavelength of 290 nm, which can be regarded as the ligand-based emission.[59] A blue shift by 55 nm was observed in the fluorescence spectra of **Zn-bdc** in the aqueous phase compared to that of the solid phase (Fig. S8, ESI†). This shift could be due to the differences in the intermolecular interactions in the solid and aqueous phase.[60] In order to explore the H_2S sensing abilities of the MOFs, an aqueous solution of Na_2S was prepared as a source of H_2S (10 μM). The quantitative detection of the H_2S by **Zn-bdc** was studied by systematically adding 2 μL portions of the aqueous Na_2S solution to the 200 μL solution of MOFs and monitoring its fluorescence. A gradual fluorescence quenching by 65 percent was observed with the addition of 10 μL of Na_2S solution (0.5 equivalents) in five portions (Fig. 3a).

The subsequent increase of Na_2S from 10 μL to 50 μL (2.5 equivalent) resulted in the enhancement of the fluorescence intensity by 4.5-fold (Fig. 4a) with respect to that MOF solution without analyte. To further increase the fluorescence intensity, the addition of Na_2S also resulted in a clear 6 nm blue shift (hypsochromic shift) that can be attributed to the nucleophilic addition of H_2S to the olefinic double bond (Fig. 4b). Furthermore, the Stern–Volmer equation ($I_0/I = 1 + K_{SV}[X]$) was used to

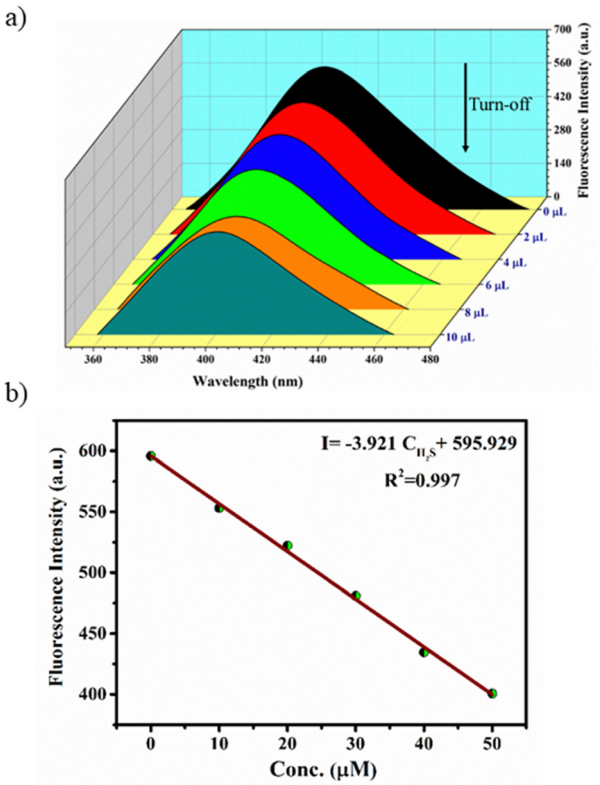

Fig. 3 (a) Fluorescence turn-off response of **Zn-bdc** upon addition of 10 μL H_2S and (b) concentration-dependent fitting curve for turn-off.

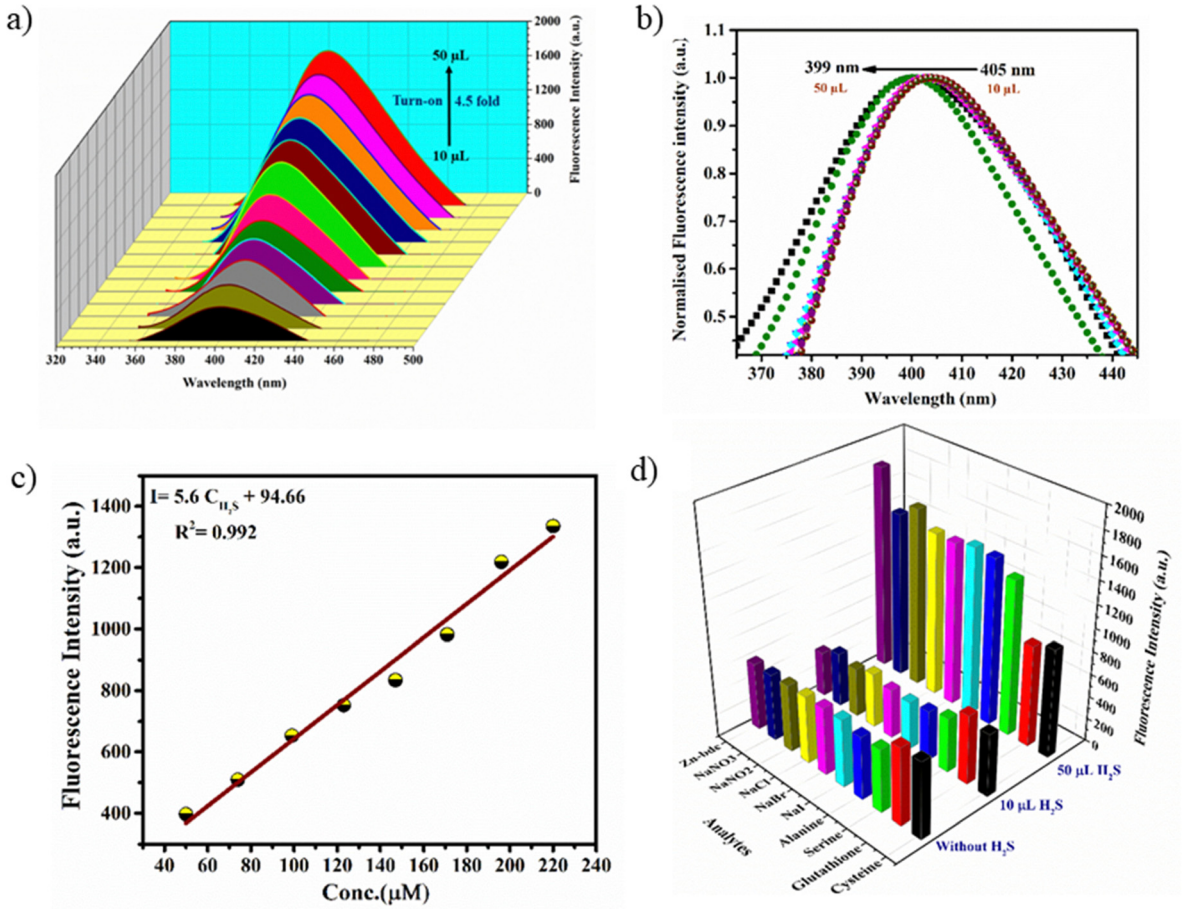

Fig. 4 (a) Turn-on fluorescence response of **Zn-bdc** upon addition of H_2S up to 50 µL, (b) blue shift of the fluorescence spectrum with turn-on, (c) concentration-dependent fitting curve for turn-on and (d) competitive fluorescence response of **Zn-bdc** towards various interfering analytes.

calculate the LOD value and quenching constant. In the equation, I_0 and I represent the fluorescence intensities of the probe before and after the addition of the analyte, respectively, [X] is the molar concentration of the H_2S solution, and K_{SV} is the quenching constant (M^{-1}) (Fig. S9, ESI†). These calculations reveal that **Zn-bdc** exhibits a quenching constant (K_{SV}) of 9.747×10^3 M^{-1} and the LOD for turn-off is 15.3 µM (Fig. 3b). For the turn-on measurements, the calibration curve showed a perfect linear relationship with the correlation coefficient R^2 of 0.99. The slope was calculated to be 5.6 with an intercept of 94.66 from the calibration curve. Therefore, using this slope (S) and the standard deviation (δ), which was calculated by measuring the fluorescence five times with a blank solution, the LOD ($3\delta/S$) for **Zn-bdc** towards sulfide was estimated to be 10.7 µM (Fig. 4c). A time-dependent fluorescence experiment with **Zn-bdc** reveals the increase of the fluorescence by 5.6-fold within 18 min for 50 µL of H_2S (Fig. S10, ESI†). Along similar lines, the H_2S sensing experiments were carried out with **Zn-btc**. It also exhibited turn-off fluorescence with the gradual addition of 10 µL of H_2S solution. However, **Zn-btc** was not found to show any turn-on fluorescence spectra even after the addition of 50 µL of H_2S (Fig. S11, ESI†). Due to the lower selectivity and sensitivity of **Zn-btc** towards H_2S, further detailed investigation was performed with the **Zn-bdc** MOF.

The sensing medium contains multiple analytes in real-life sensing experiments. Therefore, the selectivity towards the target analyte over other intrusive biomolecules is a very important aspect to consider the probe as a smart sensor. Thus, the selective detection of H_2S by **Zn-bdc** in the presence of other interfering biomolecules, such as cysteine, serine, glutathione, and alanine, and also in the presence of usual biological reducing anions, such as NaCl, NaBr, NaI, $NaNO_2$, and $NaNO_3$, was examined. All fluorescence analyses were performed in the same conditions as above with the presence of other competitive analytes. The fluorescence spectra showed significant fluorescence turn-off and turn-on also with the presence of other interfering biomolecules (Fig. S12, ESI†). In conclusion, **Zn-bdc** as a fluorescence chemosensor is selective towards H_2S in an aqueous medium with the presence of other congeners (Fig. 4d).

To ascertain the H_2S sensing mechanism and framework stability, the X-ray powder diffraction (XRPD), fluorescence resonance energy transfer (FRET), Fourier transform infrared spectroscopy (FTIR), time-correlated single photon counting (TCSPC), nuclear magnetic resonance spectroscopy (^{1}H-NMR),

and X-ray photoelectron spectroscopy (XPS) analyses were performed. The XRPD pattern of **Zn-bdc** after the addition of H_2S remains to be same as that of as-synthesized **Zn-bdc** (Fig. S13, ESI†) indicating the phase stability of the material. Notably, the emission spectrum of the **Zn-bdc** probe was found to be overlapped with the absorption spectra of the aqueous Na_2S solution, which indicates possible energy transfer between the analytes and the host (Fig. S14, ESI†).[60,61] Therefore, the initial fluorescence turn-off can be attributed to the interaction of Na_2S with **Zn-bdc** in the solution phase. The fluorescence lifetime measurement was performed by monitoring the fluorescence decay profile in the presence and absence of analyte H_2S (Fig. S15, ESI†). The excited state lifetime of **Zn-bdc** is found to be 0.24 ns in the absence of an analyte. No effective overlap was observed in the fluorescence lifetime measurement curves before and after the addition of 10 μL of H_2S to the probe solution, which may imply a dynamic quenching effect. Further addition of H_2S up to 50 μL increased the fluorescence lifetime by 8.7 times due to the fluorescence turn-on. FTIR spectra were analysed for understanding the sensing mechanism of H_2S by **Zn-bdc**. In FTIR, the disappearance of the characteristic peak of C=C of **BP3YF** at 1665 cm^{-1} was observed upon the addition of 50 μL of H_2S (Fig. S16a and b, ESI†). This indicates the nucleophilic addition of SH^- to the olefinic double bond of **BP3YF** of **Zn-bdc**. Furthermore, the appearance of a peak at 630 cm^{-1} indicates the presence of a C–S bond.[62] Furthermore, a peak around 2895 cm^{-1} appeared indicating the presence of a –SH group that is added to the olefinic carbon atom. In ^{1}H-NMR (Fig. S17 and S18, ESI†), a peak at 6.9 ppm disappeared after the treatment of H_2S indicating the nucleophilic addition to the olefinic double bond. Furthermore, the peaks of the aromatic moiety were found to shift around 7–9 ppm due to the addition of –SH to the olefin. These analyses suggest that the H_2S sensing mechanism by the MOF occurs through H_2S addition to the double bond of **BP3YF** in **Zn-bdc**. Furthermore, the XPS analysis on MOF-bdc was carried out before and after the H_2S sensing experiments to analyses the changes in the elemental composition. The as-synthesized MOF-bdc displays the signals corresponding to Zn, C, N, and O in the full-survey spectrum, whereas the presence of S was observed after the treatment with H_2S (Fig. S19a, ESI†). The Zn 2p peaks were observed at 1021.36 eV and 1044.65 eV for $2p_{3/2}$ and for $2p_{1/2}$, respectively, both in as-synthesized and H_2S-treated MOFs indicating no interaction of H_2S with Zn(II) (Fig. S19b, ESI†). The C 1s spectra for the as-synthesized MOF can be deconvoluted into three peaks at the binding energies of 284.30 eV, 285.30 eV, and 287.30 eV corresponding to the C=C, C=O, and C–O, respectively. For the H_2S-treated MOF, these three peaks were found to be slightly shifted to 284.10 eV, 285.10 eV, and 287.49 eV as well a new peak appeared at 286.48 eV corresponding to the C–S bond (Fig. S19c, ESI†).[63,64] The high-resolution spectra of S 2p were deconvoluted into two peaks at 160.67 eV and 162.05 eV, which can be marked for S $2P_{3/2}$ and S $2P_{1/2}$ splitting (Fig. S19f, ESI†). Therefore, these studies indicate the nucleophilic addition to the olefinic double bond of **Zn-bdc** by SH^-. In summary, formation of the new C–S bond in the MOF could be the probable reason for fluorescence turn-on.

Table 1 Determination of H_2S in real water samples by the standard addition method

Samples		Added (μM)	Found (μM)	Recovery (%)	RSD (%)
Tap water	1	100	99.92	99.92	4.98
	2	150	152.78	99.87	5.12
	3	200	193.74	96.87	3.42
Lake water	1	100	99.67	99.67	4.63
	2	150	147.13	98.08	2.33
	3	200	200.15	100.07	2.80
River water	1	100	96.10	96.10	5.18
	2	150	146.37	97.58	4.30
	3	200	188.65	94.32	3.22

A substantial quantity of H_2S is being released every day into water in the form of waste by the pulp and paper industry, natural gas and petroleum refinery, manufacturing industries of chemicals, volcanoes, human wastes, *etc.* The excellent selectivity and sensitivity of **Zn-bdc** towards H_2S prompted us to test its sensing ability quantitatively. The real water samples are procured from the tap (lab tap water), a lake (collected from the serpentine lake of IIT Kharagpur, India), and a river (Ganga River). The samples are prepared with varied concentrations (100 μM, 150 μM, and 200 μM) of H_2S. The H_2S concentrations of these solutions were estimated using **Zn-bdc** and it was found that the estimated values are close to the original added concentrations of H_2S in those solutions (Table 1). For all the

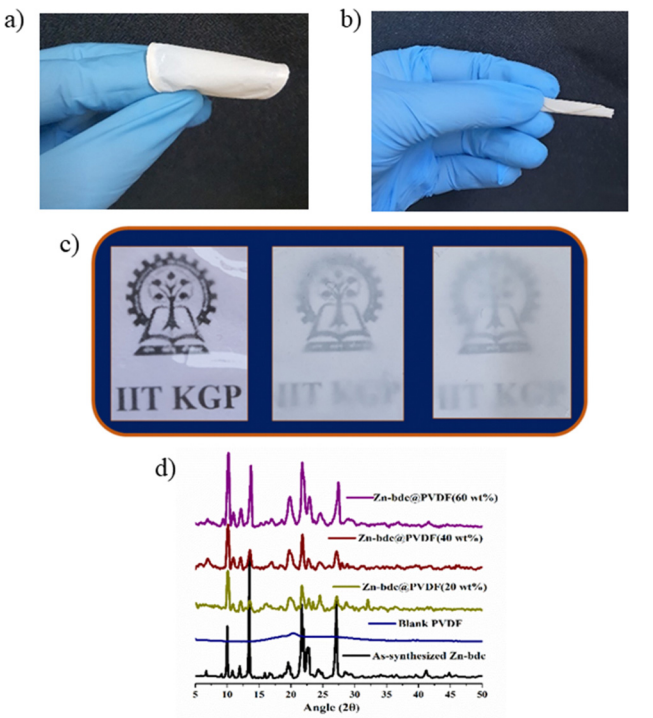

Fig. 5 (a) Optical image of the mixed-matrix membrane **Zn-bdc_60@PVDF**, (b) flexibility checking of the membrane **Zn-bdc_60@PVDF**, (c) gradual decrease of transparency of the membrane from **Zn-bdc_0@PVDF** to **Zn-bdc_40@PVDF** to **Zn-bdc_60@PVDF** and (d) XRPD patterns of the as-synthesized **Zn-bdc** and the MOF-loaded mixed-matrix membranes.

samples, the found H_2S concentrations indicate a good recovery percentage and low Relative Standard Deviation (RSD) value.[65] This result concludes that the **Zn-bdc** sensor was able to detect H_2S quantitatively from real water samples.

Detection of H_2S Gas

According to a survey by the U.S. Bureau of Labor Statistics, about 60 workers expired from 2001 to 2010 due to exposure of H_2S gas. Therefore, H_2S sensing in its gaseous phase is also as important as its detection in the solution phase.

However, most of the MOF-based probes are inadequate for the detection of H_2S in the gaseous phase. Therefore, we have explored the H_2S gas detection ability of the finely ground powdered form of the MOF and also of the MOF loaded mixed-matrix membrane.

H_2S gas detection by powdered MOF

Finely ground powder material of **Zn-bdc** was taken in two vials and placed in two wider vials containing 10 μL and 50 μL aqueous solution of Na_2S as a source of H_2S vapor. The fluorescence of the exposed material was monitored at different time intervals. No change in fluorescence intensity was observed for the material that is exposed to 10 μL of H_2S. Notably, a fluorescence turn-on phenomenon was observed with the material that is exposed to 50 μL of H_2S vapor at an excitation wavelength of 290 nm. The fluorescence intensity of the spectrum increases about 1.2-fold after the vapor deposition of H_2S for nucleophilic addition in the olefinic double bond (Fig. S22, ESI†). In summary, we can conclude that the powder form of the **Zn-bdc** probe can detect H_2S in the gaseous phase by following the nucleophilic addition mechanism.

Preparation of the mixed-matrix membrane of MOF

Rapid and selective detection of H_2S by the **Zn-bdc** probe prompted us to explore the H_2S sensing application by the mixed-matrix membrane of the MOF. The membrane was synthesized by blending the microparticles of the MOFs with PVDF in DMF solution through the slurry casting method. A total of four membranes were prepared with different loading percentages of MOFs in the membranes: **Zn-bdc_0@PVDF**, **Zn-bdc_20@PVDF**, **Zn-bdc_40@PVDF** and **Zn-bdc_60@PVDF** with 0%, 20%, 40% and 60% **Zn-bdc**, respectively (Fig. 5a).

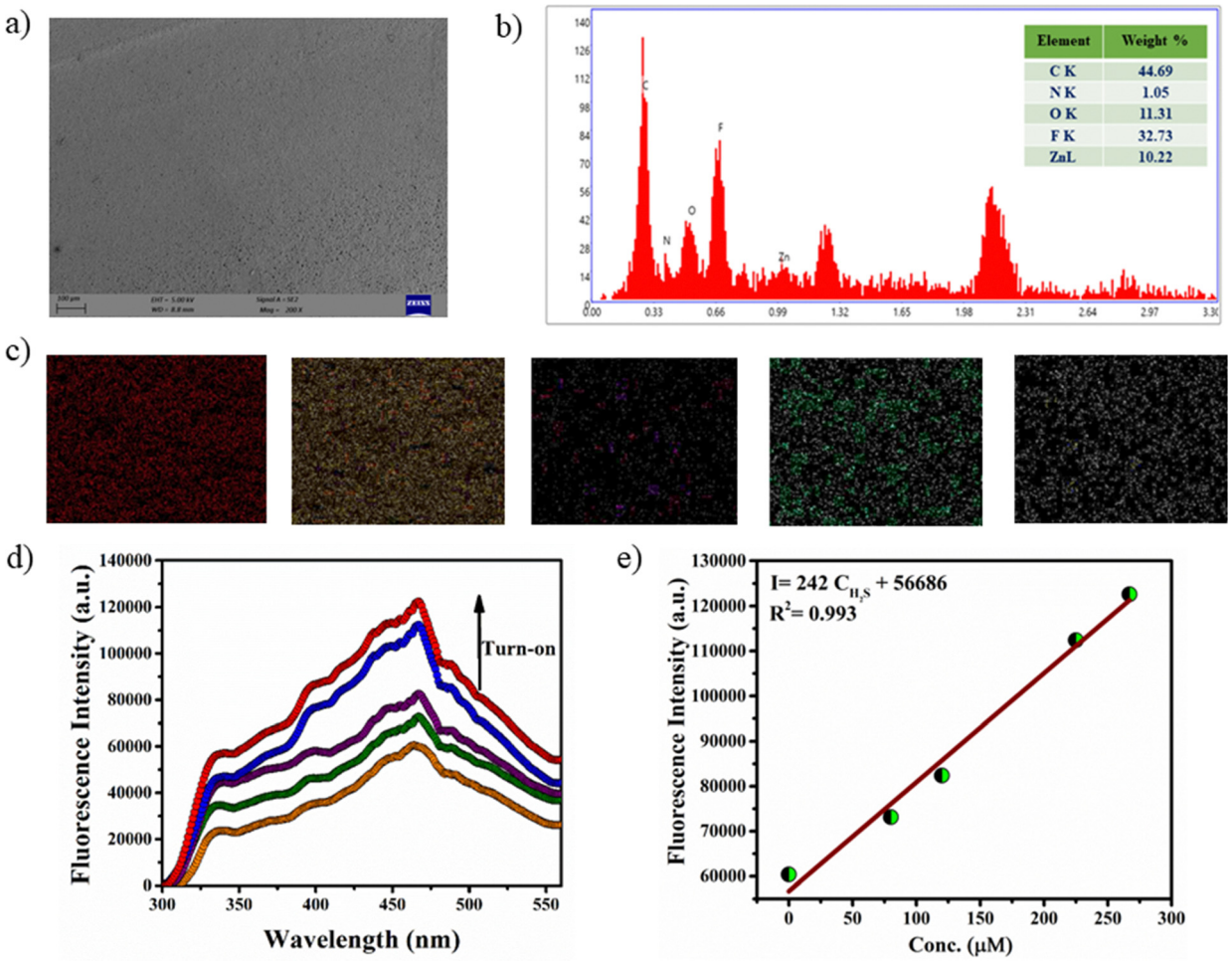

Fig. 6 (a) FESEM image, (b) EDX analysis and (c) elemental mapping (C, O, F, N, Zn) of the **Zn-bdc_60@PVDF** mixed-matrix membrane. (d) Fluorescence turn-on response of the **Zn-bdc_60@PVDF** membrane upon addition of H_2S vapor and (e) concentration dependent fitting curve for turn-on of **Zn-bdc_60@PVDF**.

Furthermore, it was found that loading of beyond 60% of **Zn-bdc** resulted in unstable membranes, which leach out the **Zn-bdc** into the DMF solution due to the lack of proper integration of the MOFs in the polymeric blend. The XRPD pattern of all four membranes was found to exhibit characteristic peaks of **Zn-bdc** (Fig. 5d) confirming the phase stability and crystallinity of the MOF in the membranes. The membranes were further characterized by field emission scanning electron microscopy (FESEM) (Fig. 6a) and energy-dispersive X-ray spectroscopy (EDX) (Fig. 6b). The elemental mapping shows a uniform distribution of carbon, nitrogen, oxygen, fluorine, and zinc, indicating the uniform dispersion of **Zn-bdc** in the composite membrane (Fig. 6c). The pure PVDF film was found to be transparent; however, the transparency of the membrane was found to decrease as the loading percentage of **Zn-bdc** increased (Fig. 5c). We would like to note here that the composite membranes are found to be mechanically robust, free of cracks, and flexible (Fig. 5b). These are some of the very important features for further application in real-time chemical sensing.

H_2S gas detection by the mixed-matrix membrane of the MOF

The H_2S sensing ability of the MOF-loaded membranes is investigated by monitoring the fluorescence of H_2S exposed membranes. The bare PVDF membrane exhibited no fluorescence and exhibited a negligible spectral change after H_2S vapor deposition, suggesting that the pure PVDF does not influence the fluorescence intensity of the H_2S detection process. Interestingly, a remarkable increase in fluorescence intensity was observed with increasing the loading percentage of **Zn-bdc** in the membranes (Fig. S23, ESI†). More interestingly, **Zn-bdc_60@PVDF** showed more pronounced fluorescence enhancement upon H_2S vapor treatment, and hence 60% film loading was selected for further investigation in detail. Similar to the solution detection, fluorescence turn-on was observed with the incremental addition of H_2S vapor (Fig. 6d). As described earlier, the nucleophilic addition reaction to the olefinic bond of the ligand is responsible for the turn-on fluorescence. Furthermore, the calibration curve for turn-on shows a perfect linear relationship with the correlation co-efficient R^2 0.99. From the linear fitted curve, the calculated slope value was 242 with an intercept of 56 686 (Fig. 6e). By using the slope value (S) and the standard deviation, which is calculated with five times blank fluorescence measurements (δ) using the PVDF film, the value of detection limit (LOD = $3\delta/S$) of **Zn-bdc_60@PVDF** toward sulfide (S^{2-}) was calculated to be 5.3 μM. Interestingly, the LOD value of the **Zn-bdc_60@PVDF** membrane is considerably lower than that of the **Zn-bdc** in

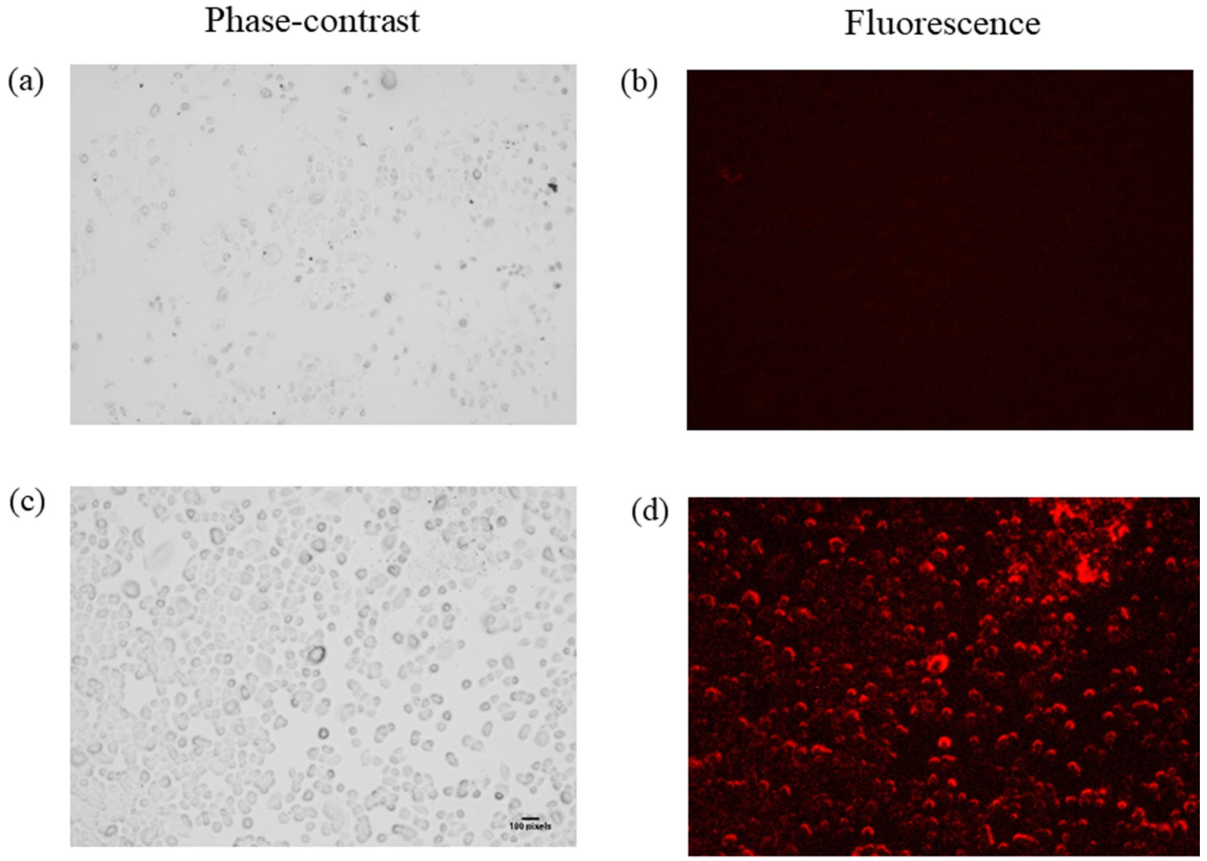

Fig. 7 Intracellular behavior of the **Zn-bdc** probe in LN-18 glioblastoma living cells: (a) phase contrast image of probe-loaded cells before H_2S treatment, (c) phase contrast image of probe-loaded cells after H_2S treatment, (b) fluorescence image of the probe-loaded respective cells before H_2S treatment and (d) fluorescence image of the probe-loaded cells after H_2S treatment.

aqueous solution. We note here that this LOD value is the lowest among all the reported Zn-based probes to date.

In vitro cell imaging of LN-18 glioblastoma cells

The fast response, excellent selectivity, and sensitivity of **Zn-bdc** towards extracellular H_2S in an aqueous medium motivated us to investigate the detection ability of **Zn-bdc** for intracellular H_2S. In this regard, cellular imaging was investigated by LN-18 glioblastoma cells in a biological medium. For a live cell imaging study of a probe, it is important to test the biocompatibility of the cell. Therefore, cytotoxicity assay analysis was performed, and the percentage of cell viability was plotted against the dose concentration of **Zn-bdc**, from which fifty percent cell growth inhibition (IC50) was calculated at 98.38 μM (Fig. S26, ESI†). The cellular morphology of the LN-18 glioblastoma cell remained intact with the different probe concentrations even after 48 hours of incubation. These results suggest that **Zn-bdc** can be considered a convenient probe for conducting cellular imaging analysis. Thus, no fluorescence was detected when cells were treated with the probe at the concentration of 98.38 μM. However, when 10 μM Na_2S solution was added as a source of endogenous H_2S and the cells were incubated for 48 hours in that solution a signal of bright red fluorescence was observed in LN-18 glioblastoma cells while maintaining their entire morphology (Fig. 7). In brief, **Zn-bdc** proved itself to be an excellent potential aspirant for *in vitro* cell imaging.

Conclusion

In conclusion, herein, three Zn(II) MOFs containing acryl-amide functionalized bis pyridyl ligands and different polycarboxylates are synthesized and structurally characterized. Two of the three MOFs (**Zn-bdc** & **Zn-btc**) were found to exhibit water stability and their utility towards H_2S sensing was explored in detail. These studies reveal that **Zn-bdc** has better H_2S sensing ability in terms of sensitivity, selectivity and stability, and exhibits turn-off and subsequent turn-on fluorescence upon exposure with the gradual addition of H_2S in the solution phase. The detection limits for **Zn-bdc** are found to be 10.7 μM in the solution phase for the nucleophilic addition. The real-time application of the MOF in a device has been demonstrated by synthesizing a mixed-matrix membrane of the **Zn-bdc** MOF using PVDF binder. Interestingly, the MOF as a film offers a brand-new sensing platform with improved permeation fluxes and contact area with the analyte. The 60% **Zn-bdc** MOF-loaded membrane exhibited highly sensitive (5.3 μM) and selective sensing capacity for gaseous phase H_2S detection. The mechanism of sensing has been established by characterizing the resultant chemical changes in the MOF upon exposure to H_2S. These studies reveal that the sensing mechanism operates through the nucleophilic addition of H_2S to the olefinic double bonds of the **BP3YF** of the MOF. Furthermore, it was also shown that the MOFs are useful for biomedical imaging as they produce red fluorescence in LN-18 glioblastoma cells upon exposure to H_2S. These results reveal that the incorporation of the MOF into mixed-matrix membranes results in an increase in the sensitivity of H_2S detection by the MOF.

Conflicts of interest

There are no conflicts to declare.

Acknowledgements

We acknowledge the financial support from DST-SERB (CRG/2022/000606), New Delhi, India, and DST-FIST for providing the single-crystal X-ray diffractometer. MDD thanks CSIR for the research fellowship. MM acknowledges the Indian Council of India, New Delhi, UGC, Govt of India, and SERB India for providing the JC Bose Fellowship.

References

1 D. J. Wales, J. Grand, V. P. Ting, R. D. Burke, K. J. Edler, C. R. Bowen, S. Mintovab and A. D. Burrows, *Chem. Soc. Rev.*, 2015, **44**, 4290.
2 H. Wang, W. P. Lustig and J. Li, *Chem. Soc. Rev.*, 2018, **47**, 4729.
3 R. J. Reiffenstein, W. C. Hulbert and S. H. Roth, *Annu. Rev. Pharmacol. Toxicol.*, 1992, **32**, 109.
4 T. L. Guidotti, *Int. J. Toxicol.*, 2010, **29**, 569.
5 H. Peng, Y. Cheng, C. Dai, A. L. King, B. L. Predmore, D. J. Lefer and B. A. Wang, *Angew. Chem., Int. Ed. Engl.*, 2011, **50**, 9672.
6 K. Eto, T. Asada, K. Arima, T. Makifuchi and H. Kimura, *Biochem. Biophys. Res. Commun.*, 2002, **293**, 1485.
7 C. Szabo, *Antioxid. Redox Signaling*, 2012, **17**, 68.
8 V. Vitvitsky and R. Banerjee, *Methods Enzymol.*, 2015, **554**, 111.
9 N. Sharma, V. Kumar and A. Jose, *Dalton Trans.*, 2023, **52**, 675.
10 J. Cui, Y.-L. Wong, M. Zeller, A. D. Hunter and Z. Xu, *Angew. Chem., Int. Ed.*, 2014, **53**, 14438.
11 M. G. Choi, S. Cha, H. Lee, L. Jeon and S. K. Chang, *Chem. Commun.*, 2009, 7390.
12 N. S. Lawrence, J. Davis, L. Jiang, T. G. J. Jones, S. N. Davies and R. G. Compton, *Electroanalysis*, 2000, **12**, 1453.
13 F. Wang, L. Wang, X. Chen and J. Yoon, *Chem. Soc. Rev.*, 2014, **43**, 4312.
14 D. Wu, A. C. Sedgwick, T. Gunnlaugsson, E. U. Akkaya, J. Yoon and T. D. James, *Chem. Soc. Rev.*, 2017, **46**, 7105.
15 D. Cao, Z. Liu, P. Verwilst, S. Koo, P. Jangjili, J. S. Kim and W. Lin, *Chem. Rev.*, 2019, **119**, 10403.
16 S. Nath, S. K. Pathak, B. Pradhan, R. K. Gupta, K. A. Reddy, G. Krishnamoorthy and A. S. Achalkumar, *New J. Chem.*, 2018, **42**, 5382.
17 W. Sun, S. Guo, C. Hu, J. Fan and X. Peng, *Chem. Rev.*, 2016, **116**, 7768.

18 F. Yu, X. Han and L. Chen, *Chem. Commun.*, 2014, **50**, 12234.
19 N. Kumar, V. Bhalla and M. Kumar, *Coord. Chem. Rev.*, 2013, **257**, 2335.
20 V. S. Lin and C. J. Chang, *Curr. Opin. Chem. Biol.*, 2012, **16**, 595.
21 B. Peng and M. Xian, *Asian J. Org. Chem.*, 2014, **3**, 914.
22 M. Strianese and C. Pellecchia, *Coord. Chem. Rev.*, 2016, **318**, 16.
23 M. Strianese, M. Lamberti and C. Pellecchia, *Dalton Trans.*, 2018, **47**, 17392.
24 M. Strianese, D. Guarnieri, M. Lamberti, A. Landi, A. Peluso and C. Pellecchia, *Inorg. Chem.*, 2020, **59**, 15977.
25 T. Xu, P. Zhang, F. Cui, J. Li, L. Kan, B. Tang, X. Zou, Y. Liu and G. Zhu, *Adv. Mater.*, 2023, **35**, 2204553.
26 Q. Yang, S. Vaesen, F. Ragon, A. D. Wiersum, D. Wu, A. Lago, T. Devic, C. Martineau, F. Taulelle, P. L. Llewellyn, H. Jobic, C. Zhong, C. Serre, G. D. Weireld and G. A. Maurin, *Angew. Chem., Int. Ed.*, 2013, **52**, 10316.
27 H. Zhang, Y. Muhammad, X. Cui, Z. Zhang, L. Liu, Z. Chu, J. Li, Y. Zhang, S. J. Shah and Z. Zhao, *J. Mater. Chem. A*, 2021, **9**, 4066.
28 D. D. Borges, P. Normand, A. Permiakova, R. Babarao, N. Heymans, D. S. Galvao, C. Serre, G. D. Weireld and G. Maurin, *J. Phys. Chem. C*, 2017, **121**, 26822.
29 G. Benedetto, B. M. Cleary, C. T. Morrell, C. G. Durbin, A. L. Brinks, J. Tietjen and K. A. Mirica, *J. Chem. Educ.*, 2023, **100**, 1289.
30 A. A. Sapianik, E. R. Dudko, K. A. Kovalenko, M. O. Barsukova, D. G. Samsonenko, D. N. Dybtsev and V. P. Fedin, *ACS Appl. Mater. Interfaces*, 2021, **13**, 14768.
31 K. Biradha, A. Goswami, R. Moi and S. Saha, *Dalton Trans.*, 2021, **50**, 10655.
32 A. H. Assen, O. Yassine, O. Shekhah, M. Eddaoudi and K. N. Salama, *ACS Sens.*, 2017, **2**, 1294.
33 S. Fajal, P. Samanta, S. Dutta and S. K. Ghosh, *Inorg. Chim. Acta*, 2020, **502**, 119359.
34 S. Tripathi and G. Anantharaman, *CrystEngComm*, 2015, **17**, 2754.
35 S. K. Sachan and G. Anantharaman, *Inorg. Chem.*, 2022, **61**, 18340.
36 W. Li, X. Yu, Y. Tang, Z. Li, S. J. Shah, Y. Liu, H. Zhao, M. Song, J. Li, G. Wang, L. Zhou, Z. Zhao, S. Liu and Z. Zhao, *Sens. Actuators, B*, 2023, **390**, 133954.
37 D. I. Pavlov, X. Yu, A. A. Ryadun, V. P. Fedin and A. S. Potapov, *Chemosensors.*, 2023, **11**, 52.
38 A. E. Thorarinsdottir and D. T. Harris, *Chem. Rev.*, 2020, **120**, 8716.
39 C. Pagis, M. Ferbinteanu, G. Rothenberg and S. Tanase, *ACS Catal.*, 2016, **6**, 6063.
40 S. Li, T. Wang, D. Tang, Y. Yang, Y. Tian, F. Cui, J. Sun, X. Jing, D. S. Sholl and G. Zhu, *Adv. Sci.*, 2022, **9**, 2203712.
41 H. Min, Z. Han, M. Wang, Y. Li, T. Zhou, W. Shi and P. Cheng, *Inorg. Chem. Front.*, 2020, **7**, 3379.
42 L. Guan, Z. Jiang, Y. Cui, Y. Yang, D. Yang and G. Qian, *Adv. Opt. Mater.*, 2021, **9**, 2002180.
43 S. S. Nagarkar, B. Joarder, A. K. Choudhari, S. Mukherjee and S. K. Ghosh, *Angew. Chem., Int. Ed.*, 2013, **52**, 2881.
44 X. Zhang, Q. Hu, T. Xia, J. Zhang, Y. Yang, Y. Cui, B. Chen and G. Qian, *ACS Appl. Mater. Interfaces*, 2016, **8**, 32259.
45 S. Nandi, H. Reinsch and S. Biswas, *Microporous Mesoporous Mater.*, 2020, **293**, 109790.
46 Y. Li, X. Zhang, L. Zhang, K. Jiang, Y. Cui, Y. Yang and G. Qian, *J. Solid State Chem.*, 2017, **255**, 97.
47 H. Yu, C. Liu, Y. Li and A. Huang, *ACS Appl. Mater. Interfaces*, 2019, **11**, 41972.
48 H. Li, X. Feng, Y. Guo, D. Chen, R. Li, X. Ren, X. Jiang, Y. Dong and B. Wang, *Sci. Rep.*, 2014, **4**, 4366.
49 S. Saha, P. K. Roy, K. Maity, M. Mandal and K. Biradha, *Chem. – Eur. J.*, 2021, **28**, e202103830.
50 X. Zhang, Q. Zhang, D. Yue, J. Zhang, J. Wang, B. Li, Y. Yang, Y. Cui and G. Qian, *Small*, 2018, **14**, 1801563.
51 X. Han, J. Liu, K. Yu, Y. Lu, W. Xiang, D. Zhao and Y. He, *Inorg. Chem.*, 2022, **61**, 5067.
52 S. G. Surya, S. Bhanoth, S. M. Majhi, Y. D. More, V. M. Teja and K. N. Chappanda, *CrystEngComm*, 2019, **21**, 7303.
53 S. S. Nagarkar, A. V. Desai and S. K. Ghosh, *Chem. – Eur. J.*, 2015, **21**, 9994.
54 S. H. Hosseini-Shokouh, J. Zhou, E. Berger, Z. P. Lv, X. Hong, V. Virtanen, K. Kordas and H. P. Komsa, *ACS Appl. Mater. Interfaces*, 2023, **15**, 7063.
55 X. Zheng, R. Fan, Y. Song, A. Wang, K. Xing, X. Du, P. Wang and Y. Yang, *J. Mater. Chem. C*, 2017, **5**, 9943.
56 L. Rajput, S. Singha and K. Biradha, *Cryst. Growth Des.*, 2007, **7**, 2788.
57 K. Nath, K. Maity and K. Biradha, *Cryst. Growth Des.*, 2017, **17**, 4437.
58 D. Sun, Z. H. Yan, V. A. Blatov, L. Wang and D. F. Sun, *Cryst. Growth Des.*, 2013, **13**, 1277.
59 R. Moi, K. Nath and K. Biradha, *Chem. – Asian J.*, 2019, **14**, 3742.
60 Z. W. Zhai, S. H. Yang, M. Cao, L. K. Li, C. X. Du and S. Q. Zang, *Cryst. Growth Des.*, 2018, **18**, 7173.
61 K. E. Sapsford, L. Berti and I. L. Medintz, *Angew. Chem., Int. Ed.*, 2006, **45**, 4562.
62 C. N. R. Rao, R. Venkataraghavan and T. R. Kasturi, *Can. J. Chem.*, 1964, **42**, 36.
63 A. Munir, T. u Haq, A. Qurashi, H. U. Rehman, A. U. Hamid and I. Hussain, *ACS Appl. Energy Mater*, 2019, **2**, 363.
64 D. Chen, C. Gan, X. Fan, L. Zhang, W. Li, M. Zhu and X. Quan, *Materials*, 2019, **12**, 2800.
65 D. Harvey, *Modern Analytical Chemistry*, 2000.